



OPEN ACCESS

EDITED BY

Hui Zhao,
Guangdong Ocean University, China

REVIEWED BY

Yuqiu Wei,
Chinese Academy of Fishery Sciences (CAFS),
China
Yong Zhang,
Fujian Normal University, China

*CORRESPONDENCE

Lingqi Ma
✉ lingqima@tsu.edu

[†]These authors have contributed equally to this work

RECEIVED 24 August 2024

ACCEPTED 10 September 2024

PUBLISHED 02 October 2024

CITATION

Tong Z, Wang C, Lin L, Ma L and Huang B (2024) Nutrient depletion and phytoplankton shifts driven by the Pearl River plume in the Taiwan Strait.
Front. Mar. Sci. 11:1485670.
doi: 10.3389/fmars.2024.1485670

COPYRIGHT

© 2024 Tong, Wang, Lin, Ma and Huang. This is an open-access article distributed under the terms of the [Creative Commons Attribution License \(CC BY\)](https://creativecommons.org/licenses/by/4.0/). The use, distribution or reproduction in other forums is permitted, provided the original author(s) and the copyright owner(s) are credited and that the original publication in this journal is cited, in accordance with accepted academic practice. No use, distribution or reproduction is permitted which does not comply with these terms.

Nutrient depletion and phytoplankton shifts driven by the Pearl River plume in the Taiwan Strait

Zhuyin Tong^{1†}, Changyun Wang^{1†}, Lizhen Lin², Lingqi Ma^{1,2,3*} and Bangqin Huang¹

¹State Key Laboratory of Marine Environmental Science/National Observation and Research Station for the Taiwan Strait Marine Ecosystem (T-SMART)/Fujian Provincial Key Laboratory for Coastal Ecology and Environmental Studies, Xiamen University, Xiamen, Fujian, China, ²State Key Laboratory of Marine Environmental Science/College of the Ocean and Earth Sciences, Xiamen University, Xiamen, Fujian, China, ³Department of Environmental Sciences, College of the Coast & Environment, Louisiana State University, Baton Rouge, LA, United States

The intrusion of the Pearl River plume into the Taiwan Strait provides a unique case study that challenges traditional assumptions about the impacts of nutrient-rich river plumes on coastal phytoplankton communities. In this study, we conducted a detailed analysis of nutrient dynamics and phytoplankton composition within the Taiwan Strait, focusing on the effects of the Pearl River plume. Our findings reveal significant nutrient depletion, particularly of nitrogen, in the surface waters as the plume extends seaward, resulting in nitrogen limitation and a marked reduction in phytoplankton biomass. Vertical stratification within the Taiwan Strait creates distinct ecological niches, with the mid-layer supporting a deep chlorophyll maximum and the surface layer becoming dominated by the picophytoplankton *Synechococcus*. This shift from diatom-dominated communities to *Synechococcus* dominance has far-reaching implications for carbon cycling and food web dynamics in the region. Our results suggest that the Pearl River plume's influence on the Taiwan Strait represents a departure from the typical nutrient enrichment associated with river plumes, highlighting the complexity of coastal biogeochemical processes.

KEYWORDS

Pearl River plume, phytoplankton community, nutrient limitation, Taiwan Strait, nitrogen limitation

1 Introduction

Marine phytoplankton contribute to approximately half of global primary production and play a crucial role in biogeochemical cycles (Field et al., 1998). In coastal regions, phytoplankton communities are highly dynamic and sensitive to human activities, undergoing significant alterations due to interactions within the land-ocean continuum

formed by river plumes mixing with oceanic waters (Gomes et al., 2018). Traditionally, river plumes in low-latitude regions are characterized by high temperature, low salinity, and low density (Vic et al., 2014). These plumes are usually nutrient-rich, which typically supports elevated phytoplankton biomass and productivity, particularly in areas close to the estuary (Yin et al., 2001). This prevailing view has led to the assumption that river plumes generally enhance phytoplankton growth due to their high nutrient loads.

The Pearl River, the second largest river in China, discharges substantial amounts of terrestrial material into the northern South China Sea (NSCS) (Cai et al., 2004). The Pearl River Estuary (PRE) is known for its frequent phytoplankton blooms, predominantly dominated by diatoms, which occur throughout the year (Shen et al., 2011). The occurrence of these blooms is primarily driven by the high nutrient availability in the river plume. However, additional factors, such as water column stratification and light limitation, also play a role in terminating these blooms (Lu and Gan, 2015). As the Pearl River plume extends offshore, it experiences a transition from phosphorus (P) limitation to nitrogen (N) limitation, which in turn triggers a succession of dominant phytoplankton groups on the NSCS shelf (Yin et al., 2001, 2004; Tong et al., 2023).

In recent years, the Pearl River plume has been observed occasionally intruding into the Taiwan Strait (TWS) (Bai et al., 2015). The Taiwan Strait serves as a critical channel connecting the East and South China Seas, and its summer dynamics are predominantly influenced by southwest monsoon winds. The complex flow system in this region, shaped by processes such as upwelling events (Zhong et al., 2019), coastal currents (Hong et al., 2011), and Kuroshio intrusion (Huang et al., 2015), introduces significant amounts of nutrients into the TWS (Wang et al., 2013). Long-term observations have demonstrated that the realized niches of phytoplankton groups in the TWS are strongly shaped by these dynamic environmental factors (Zhong et al., 2020). However, despite the recognized importance of the Pearl River plume, studies on its specific impact on the phytoplankton dynamics within the Taiwan Strait remain limited.

Existing research has identified significant impacts of the Pearl River plume on the phytoplankton community composition in the NSCS shelf region. For example, previous studies have shown that the intrusion of the Pearl River plume can lead to extensive phytoplankton blooms, altering the ecological dynamics of the receiving waters (Dai et al., 2008; Han et al., 2012). However, when the plume extends into the Taiwan Strait, the scenario becomes more complex. The nutrient content of the plume, particularly nitrogen, tends to be significantly depleted as it travels farther from its source, potentially altering the expected positive influence on phytoplankton biomass (Han et al., 2012; Tong et al., 2023).

The intrusion of the Pearl River plume into the Taiwan Strait has been associated with various ecological effects. For instance, satellite observations and numerical modeling studies have reported episodes where the plume led to phytoplankton blooms across the entire TWS (Bai et al., 2015). Conversely, there have also been observations indicating that a decrease in nutrient input from river runoff, coupled with a weakening of wind-forced mixing, could lead

to a decline in chlorophyll concentrations (Gao et al., 2020). These findings suggest that the impact of the Pearl River plume on the Taiwan Strait is not straightforward and may involve complex interactions between physical and biological processes.

In this study, we conducted a 24-hour time series of observations at three stations within the Pearl River plume system in the Taiwan Strait during the summer of 2014. By integrating hydrological parameters with phytoplankton community data, our goal was to elucidate the processes and mechanisms underlying the response of the phytoplankton community to the plume in the TWS. We hypothesize that, contrary to the traditional view, the intrusion of the nutrient-depleted Pearl River plume into the Taiwan Strait may lead to a reduction in local phytoplankton biomass and a shift in community composition. Our findings are expected to contribute to a deeper understanding of the complex biogeochemical interactions within the land-ocean interface and challenge existing paradigms regarding the role of river plumes in coastal phytoplankton dynamics.

2 Materials and methods

2.1 Study areas and sample collection

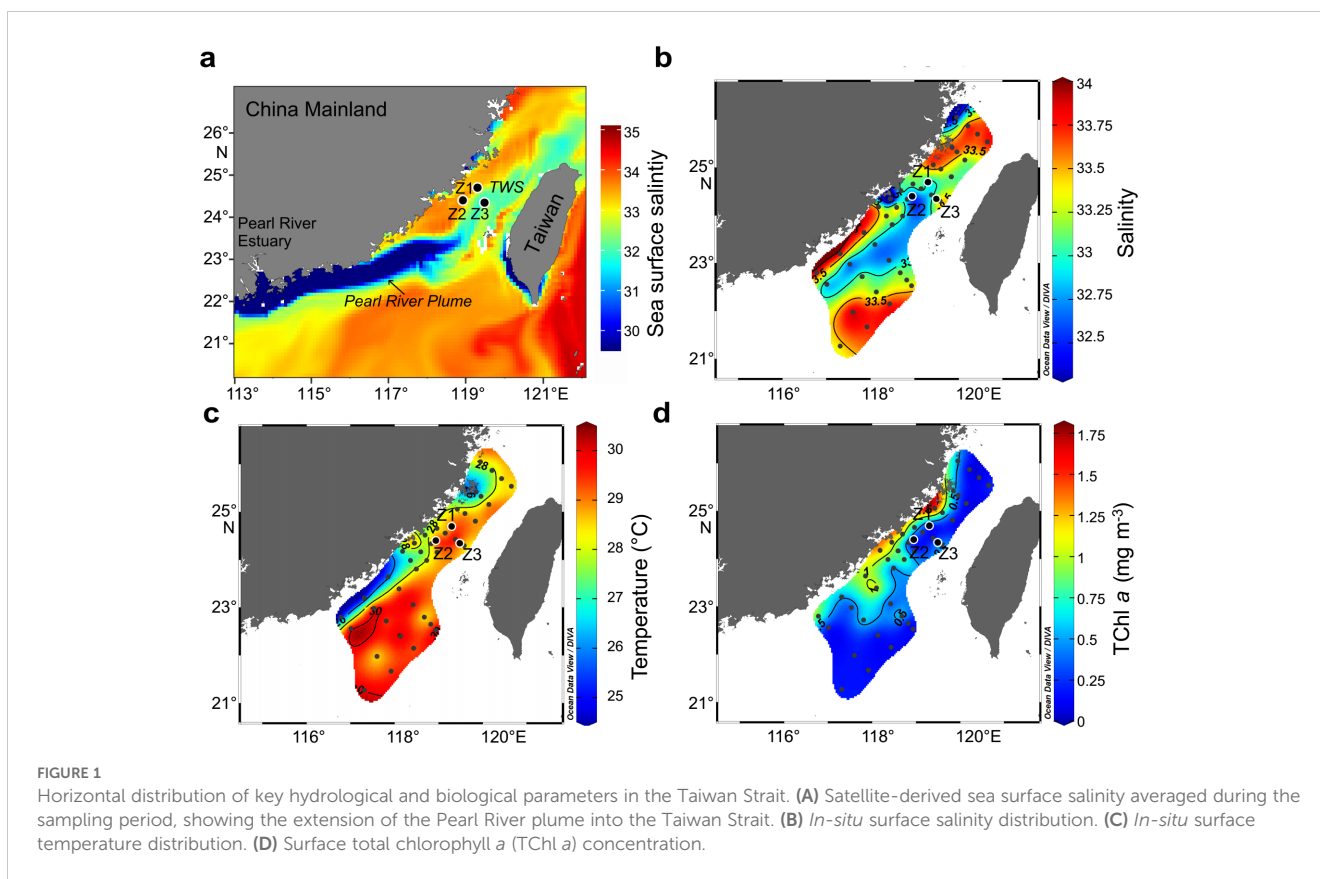
Water samples were collected aboard the R/V Yanping II from 12 July to 16 July at three 24-hour continuous observing stations (Z1, Z2, and Z3) in the Taiwan Strait (TWS). These stations were selected based on their expected interaction with the Pearl River plume, which extended into the TWS during the sampling period, significantly influencing surface salinity and other hydrological parameters at all three stations (Figure 1). Satellite sea surface salinity data were obtained from the Copernicus Marine Service (<https://marine.copernicus.eu/>) to track the plume's spatial extent.

To capture the hydrological and biological conditions across different depths influenced by the plume, water temperature, salinity, turbidity, and fluorescence were measured using a SeaBird model SBE9/11 conductivity-temperature-depth (CTD) recorder. Seawater samples were collected with Niskin bottles attached to the CTD rosette system, focusing on different depth layers to capture vertical gradients. Dissolved inorganic nutrient concentrations, including nitrogen (nitrate and nitrite, NO_x , $\mu\text{mol L}^{-1}$), phosphorous (PO_4^{3-} , $\mu\text{mol L}^{-1}$) and silicate (Si(OH)_4 , $\mu\text{mol L}^{-1}$), were analyzed using a QUAATRO nutrient analyzer. The detection limits for NO_x , PO_4^{3-} and Si(OH)_4 were 0.04, 0.02, and $0.11 \mu\text{mol}\cdot\text{L}^{-1}$, respectively. The stability of the water column stratification, represented by the squared Brunt-Väisälä frequency (N^2), was calculated following the method developed by Mourinho-Carballido et al. (2016), using the equation:

$$N^2 = \left(\frac{g}{\rho}\right)\left(\frac{\partial \rho}{\partial z}\right) \quad (1)$$

where g is the gravitational acceleration (9.81 m s^{-2}), ρ is the potential density of water (kg m^{-3}) and z is depth (m).

For this study, we focused on vertical layers within the water column: the surface layer (0–10 m), mid-layer (10–20 m), and bottom layer (below 20 m), based on salinity and temperature gradients observed in the CTD profiles. These layers represent the



different degree of interaction between the Pearl River plume and the ambient seawater, with the surface layer being most influenced by the plume's low salinity and high temperature characteristics.

The thickness of the plume-influenced surface layer was determined by identifying the depth at which salinity increased to above 33 (Wu et al., 2017), marking the transition from plume-influenced water to more typical seawater characteristics. The deep chlorophyll maximum layer (DCML) was identified using fluorescence data from the CTD and typically occurred within the mid-layer, though it varied depending on local hydrodynamic conditions.

2.2 Phytoplankton biomass and community analysis

Phytoplankton pigment samples were collected at multiple depths within each station to capture the vertical distribution of phytoplankton communities. Seawater volumes of 4–10 L were collected and filtered through 25-mm GF/F filters (Whatman) under less than 50 mmHg pressure. Filters were immediately stored in liquid nitrogen and later transferred to a -80°C freezer for analysis in the laboratory. Photosynthetic pigments were extracted using N, N-dimethylformamide and mixed with isopycnic ammonium acetate in brown chromatographic bottles. The pigment composition was analyzed using high-performance liquid chromatography (HPLC) with a 3.5 μm Eclipse XDB C8 column, based on the quantification of standards provided by Danish Hydraulic Institute (DHI) Water and Environment,

Hørsholm, Denmark. The measurement procedures followed those detailed in previous studies (Xiao et al., 2018).

To determine the absolute and relative abundance of nine phytoplankton groups—including dinoflagellates, diatoms, haptophytes_T8, haptophytes_T6, chlorophytes, cryptophytes, *Prochlorococcus*, *Synechococcus*, and prasinophytes—we used the CHEMTAX program, which derives these abundances from thirteen diagnostic pigments associated with fractions of the TChl *a* pool. The initial pigment/Chl *a* ratios for each phytoplankton class were based on values validated in previous studies (Wang et al., 2015). Successive runs of CHEMTAX were performed to achieve convergence between input and output ratios (Latasa, 2007).

2.3 Statistical analysis

All data were analyzed using R software version 4.2.2 (R Core Team, 2022). The non-parametric pairwise Wilcoxon test was employed for *post hoc* analysis to identify statistical differences in nutrient concentrations, nutrient ratios, and phytoplankton biomass across different vertical layers. To explore the relationships between dominant phytoplankton groups and key environmental variables, we used canonical correspondence analysis (CCA) implemented in the “vegan” package. Additionally, univariate generalized additive models (GAMs) were developed using the “mgcv” package to assess the influence of environmental variables on phytoplankton biomass, with the model defined as:

$$Y = \alpha + s(x) + \varepsilon \quad (2)$$

where Y represents phytoplankton biomass. The term $s(x)$ indicates a one-dimensional nonlinear function based on cubic regression splines, and x represents one of the predictors (including salinity, NO_x , PO_4^{3-} , $\text{Si}(\text{OH})_4$, N:P, and Si:N). The terms α and ε represent the intercept of the model and the residual error, respectively.

3 Results

3.1 Hydrological characteristics

Temperature, salinity, turbidity and buoyancy frequency squared (N^2) exhibited distinct vertical distributions across the 24-hour time-series observations at stations Z1, Z2, and Z3 (Figure 2). At all three stations, the surface layer, influenced by the Pearl River plume, was characterized by low salinity (32.34–33), low turbidity (0.45–0.68 FTU), and high temperature (28.64–30.29°C). The mid-layer, which represented the mixing zone between plume-influenced surface water and the underlying seawater, displayed intermediate hydrological properties, with temperature, salinity, and turbidity ranging from

25.1–29.4°C, 33–34 and 0.56–3.32 FTU, respectively. The bottom layer, corresponding to deeper seawater, was marked by lower temperature (23.76–26.81°C), higher salinity (34–34.35), and higher turbidity (1.82–18.00 FTU).

At station Z1, a clear double stratification was observed at 10–20 m and 40–50 m depths, distinguishing different layers of water within the column. At station Z2, the plume became shallower over time, with the depth of maximum N^2 consistent with the plume's depth. At station Z3, the plume exhibited an irregular vertical structure, with deeper mixing with seawater occurring between 6–9 hours after the start of observations, resulting in a deeper stratification compared to other times during the observation period.

The vertical distribution of nutrient concentrations and ratios varied differently across the surface, mid-layer, and bottom layers at stations Z1–Z3 (Figure 3). At station Z1, NO_x , PO_4^{3-} , and $\text{Si}(\text{OH})_4$ concentrations were lowest in the surface layer and highest in the bottom layer. N:P ratios were lowest in the surface layer, whereas Si:N ratios were highest. At station Z2, NO_x and PO_4^{3-} concentrations exhibited a significant increase from the surface water to the mid-layer and bottom layer. $\text{Si}(\text{OH})_4$ concentrations did not differ significantly between the mid-layer and bottom layer. At station Z3, both NO_x and PO_4^{3-} concentrations increased significantly

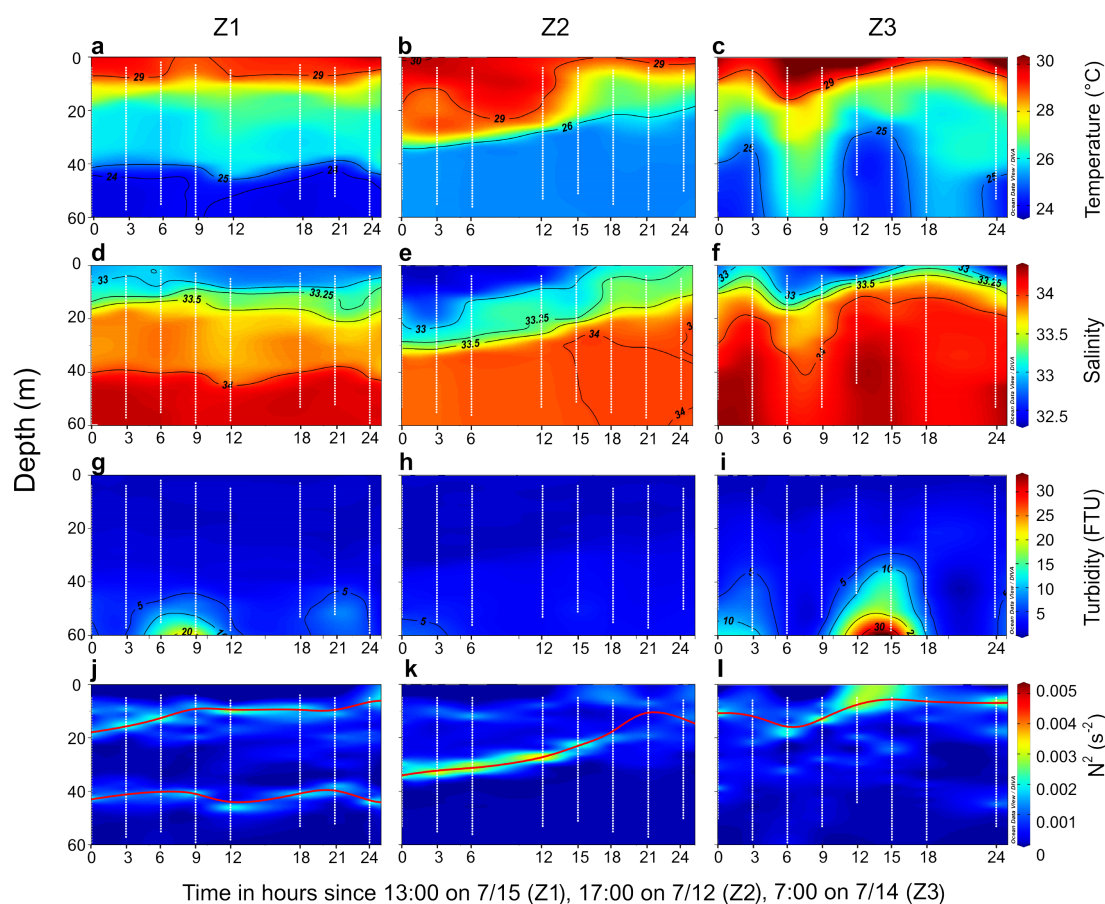


FIGURE 2

Temporal variations in vertical profiles of physical and chemical parameters at stations Z1, Z2, and Z3. Profiles of (A–C) Temperature, (D–F) salinity, (G–I) turbidity, and (J–L) buoyancy frequency squared (N^2). The red solid line indicates the depth of maximum N^2 , with two occurrences of maximum N^2 denoted by two lines at station Z1. The white dots represent sampling depths recorded by the conductivity–temperature–depth (CTD) recorder at one-meter intervals throughout the water column.

from the surface layer to the mid-layer. Across all stations, the mean values of NO_x ($0.39 \pm 0.39 \mu\text{mol L}^{-1}$), PO_4^{3-} ($0.08 \pm 0.04 \mu\text{mol L}^{-1}$), Si(OH)_4 ($3.02 \pm 0.96 \mu\text{mol L}^{-1}$), and N:P (5 ± 4) were significantly lower, while Si:N (18 ± 16) was significantly higher in the surface layer compared to the mid-layer and bottom layer.

3.2 Characteristics of phytoplankton biomass and community composition

The vertical distribution of fluorescence and TChl *a* is shown in Figure 4A. The depths of maximum fluorescence concentrations were consistent with those of TChl *a*, with both exhibiting high values in the subsurface layer and lower values in the surface and bottom layers at stations Z1, Z2, and Z3. Regression analysis revealed a significant positive correlation between fluorescence and TChl *a* (Figure 4B), which supports the use of fluorescence as a proxy for TChl *a*. Accordingly, the deep chlorophyll maximum

layer (DCML) was defined as the depth of maximum fluorescence. The depth of the DCML showed a positive relationship with the thickness of the plume-influenced surface layer (Figure 4C). The concentration of TChl *a* was highest in the mid-layer ($0.73 \pm 0.23 \text{ mg m}^{-3}$), followed by the bottom layer ($0.54 \pm 0.22 \text{ mg m}^{-3}$) and the surface layer ($0.39 \pm 0.22 \text{ mg m}^{-3}$) when considering all data from stations Z1, Z2, and Z3.

The phytoplankton community composition exhibited vertical heterogeneity across different vertical layers (Figure 5). Diatoms were the dominant group in areas with high TChl *a* concentrations, particularly in the mid-layer (55%) and bottom layer (51%), but also contributed significantly in the surface layer (40%). *Synechococcus* also dominated in the surface layer (26%), while prasinophytes accounted for 17% of the TChl *a* in the mid-layer. In the bottom layer, haptophytes_T8 (12%) and *Prochlorococcus* (9%) were the dominant groups. Other non-dominant groups, including dinoflagellates, chlorophytes, cryptophytes, and haptophytes_T6, each contributed less than 3% to the total TChl *a* during the observation period.

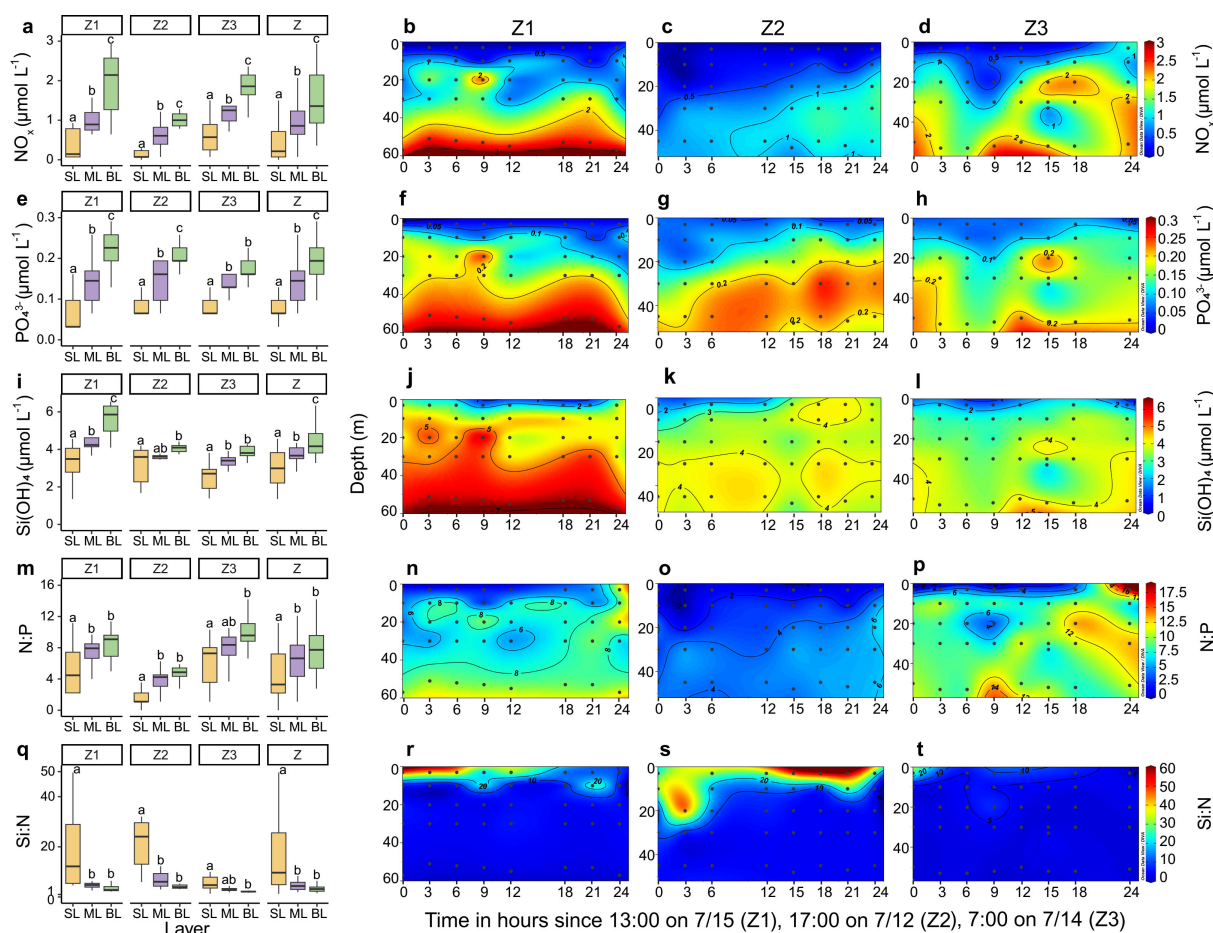


FIGURE 3

Variations in nutrient concentrations and ratios across vertical layers over time at stations Z1, Z2, and Z3. (A–D) NO_x concentrations, (E–H) PO_4^{3-} concentrations, (I–L) Si(OH)_4 concentrations, (M–P) N:P ratios, and (Q–T) Si:N ratios. The box plots show the distribution of values within each vertical layer, with boxes defining the hinge (25%–75% quartile) and the black line extending to 1.5 times the interquartile range. The black horizontal line within each box denotes the median. Differences between values for vertical layers at each station were determined by Wilcoxon tests. Letters above the boxes indicate significant differences among the vertical layers ($p < 0.05$). Z represents all data from stations Z1–Z3. SL, ML, and BL denote the surface layer, mid-layer, and bottom layer, respectively. The black dots in the transect plots denote biological sampling stations.

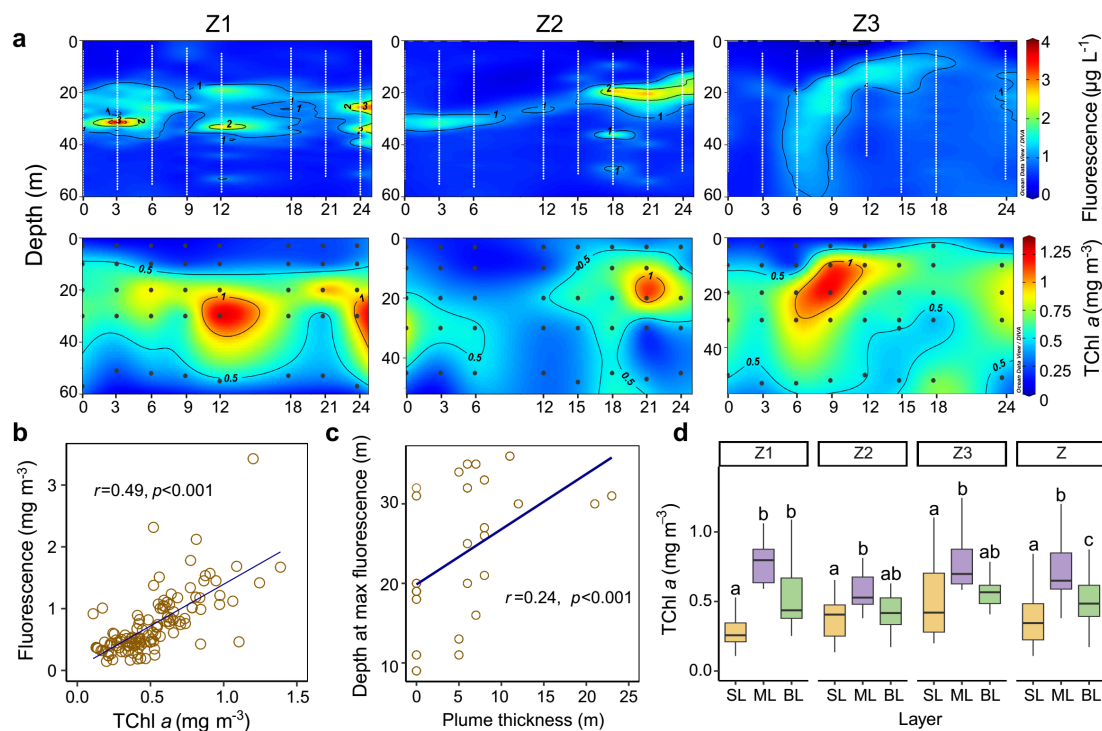


FIGURE 4

Vertical distribution and relationships of fluorescence and TChl *a* across stations Z1, Z2, and Z3. (A) Transect distribution of fluorescence and TChl *a* at stations Z1–Z3. The white dots represent sampling depths recorded by the conductivity–temperature–depth (CTD) recorder at one-meter intervals throughout the water column. (B) Relationship between fluorescence and TChl *a*. (C) Relationship between the depth of maximum fluorescence and plume-influenced layer thickness. (D) Boxplots of TChl *a* across different vertical layers at stations Z1, Z2, Z3, and Z (all data from stations Z1–Z3). Differences between values for vertical layers at each station were determined by Wilcoxon tests. Letters above the boxes indicate significant differences among the vertical layers ($p < 0.05$). SL, ML, and BL denote the surface layer, mid-layer, and bottom layer, respectively. The black dots in the transect plots denote biological sampling stations.

3.3 Temporal variability of phytoplankton biomass in relation to the effect of river plume

The temporal variations in salinity and NO_x were closely linked to changes in phytoplankton biomass at the surface of stations Z1, Z2, and Z3 during the 24-hour time-series observations (Figure 6). At station Z1, the river plume consistently covered the surface layer, resulting in a significant positive correlation between phytoplankton biomass and NO_x concentrations (Figure 6H). As mixing water progressively invaded the surface at stations Z2 and Z3, a corresponding increase in phytoplankton biomass was observed (Figures 6B–C, E–G). At station Z2 and when considering all stations collectively (Z), phytoplankton biomass exhibited a significant positive relationship with salinity (Figure 6G). However, during the 12–24 hour period at stations Z2 and Z3, a slight increase in NO_x concentrations and phytoplankton biomass was noted, but no significant correlation was found between these variables.

3.4 Relationship between phytoplankton and environmental factors

TChl *a* exhibited a unimodal relationship with NO_x and PO_4^{3-} across different vertical layers (Figures 7A, B). In the surface layer,

TChl *a* concentrations increased with NO_x (ranging mostly from 0 to $0.5 \mu\text{mol L}^{-1}$, with an outlier at $1.21 \mu\text{mol L}^{-1}$), reaching a peak when NO_x was around $1.2 \mu\text{mol L}^{-1}$ in the mid-layer, before decreasing in the bottom layer. PO_4^{3-} followed a similar trend, with the peak of fitted TChl *a* occurring when PO_4^{3-} was around $0.15 \mu\text{mol L}^{-1}$.

Phytoplankton groups displayed varied responses to environmental factors across different vertical layers (Figures 7C–F). Our emphasis was placed on five dominant groups, including diatoms, haptophytes_T8, prasinophytes, *Synechococcus*, and *Prochlorococcus*, due to their significant roles in shaping the phytoplankton biomass and community composition (Figure 5). Diatoms showed a broad adaptive range concerning temperature, salinity, turbidity, nutrient concentrations, and nutrient ratios, with a preference for areas with higher concentrations of NO_x , PO_4^{3-} , and $\text{Si}(\text{OH})_4$ (Figure 7F). Prasinophytes and *Synechococcus* preferred higher temperatures, with *Synechococcus* consistently showing a negative correlation with salinity, indicating its susceptibility to environmental changes. *Prochlorococcus* was more abundant in areas with higher turbidity, while haptophytes_T8 preferred high nutrient concentrations, although both groups thrived primarily in the bottom layer.

4 Discussion

The conventional understanding has been that low-latitude river plumes, enriched with nutrients and characterized by warm

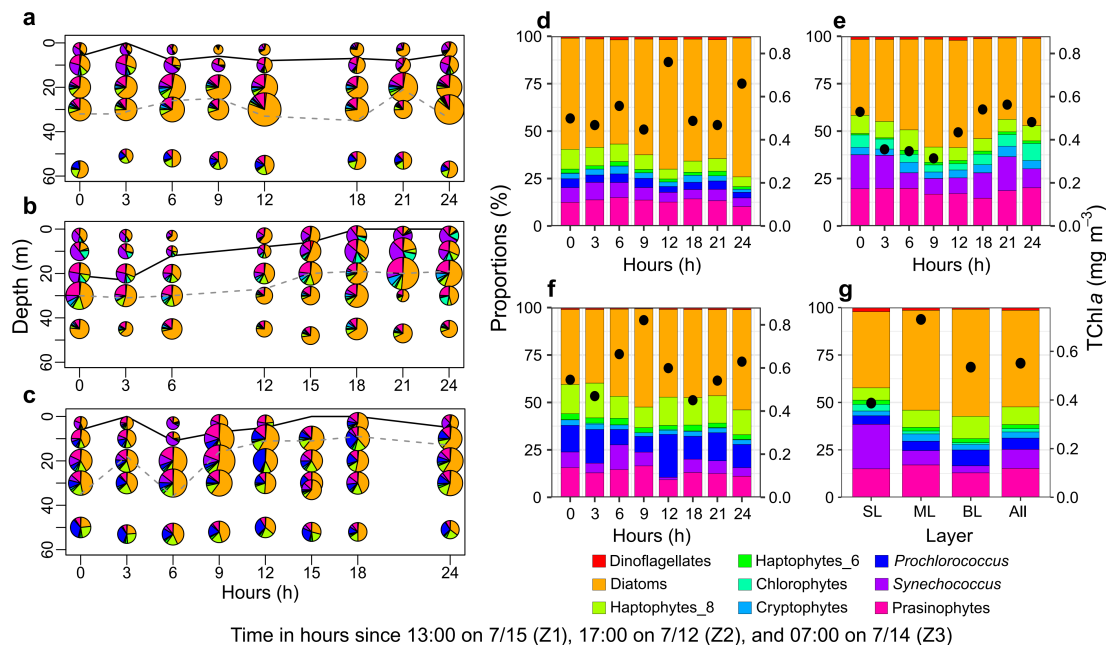


FIGURE 5

Vertical distribution and composition of phytoplankton communities across stations Z1, Z2, and Z3. (A–C) Vertical distribution of phytoplankton communities at stations Z1, Z2, and Z3. The black solid line and grey dashed line denote the thickness of the plume-influenced layer and the deep chlorophyll maximum layer, respectively. (D–F) Comparison of average depth-integrated phytoplankton biomass and community composition at stations Z1, Z2, and Z3. (G) Comparison of average phytoplankton biomass and community composition across different vertical layers and all combined data (Z) from stations Z1–Z3.

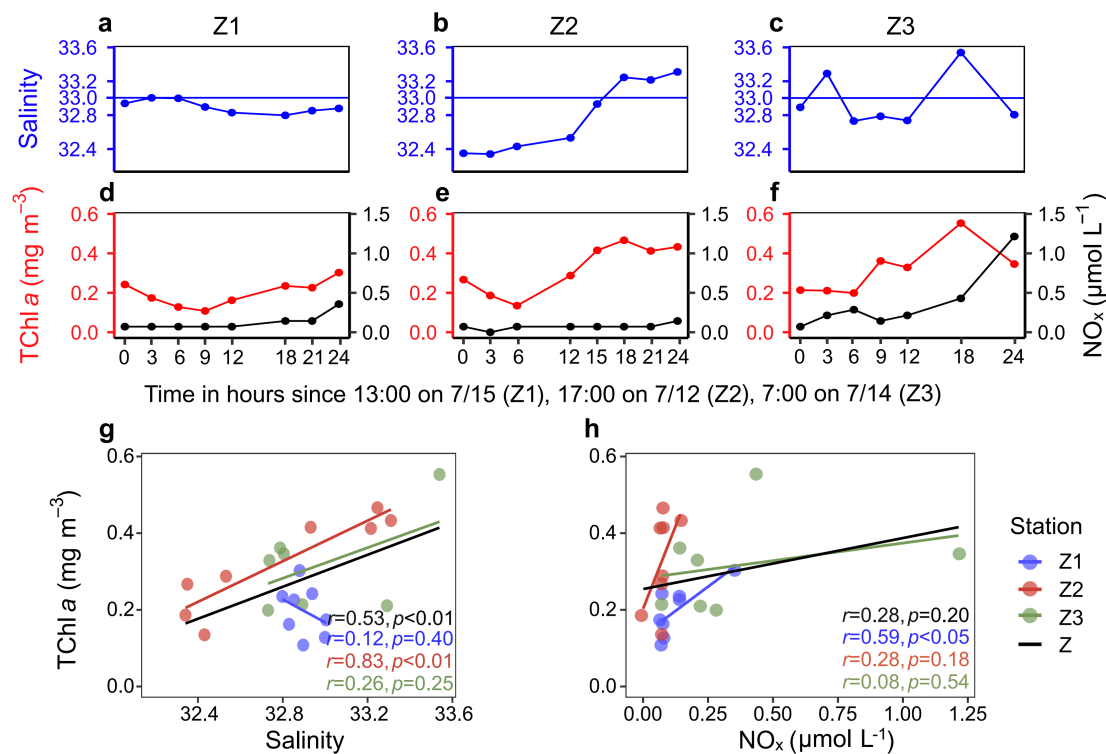


FIGURE 6

Temporal variations in salinity, phytoplankton biomass, and NO_x concentrations at the surface of stations Z1, Z2, and Z3. (A–C) Temporal variations in salinity at the surface of stations Z1, Z2, and Z3. (D–F) Temporal variations in TChla and NO_x concentrations at the surface of stations Z1, Z2, and Z3. (G) Relationship between TChla and salinity across stations Z1, Z2, Z3, and combined data (Z). (H) Relationship between TChla and NO_x concentrations across stations Z1, Z2, Z3, and combined data (Z).

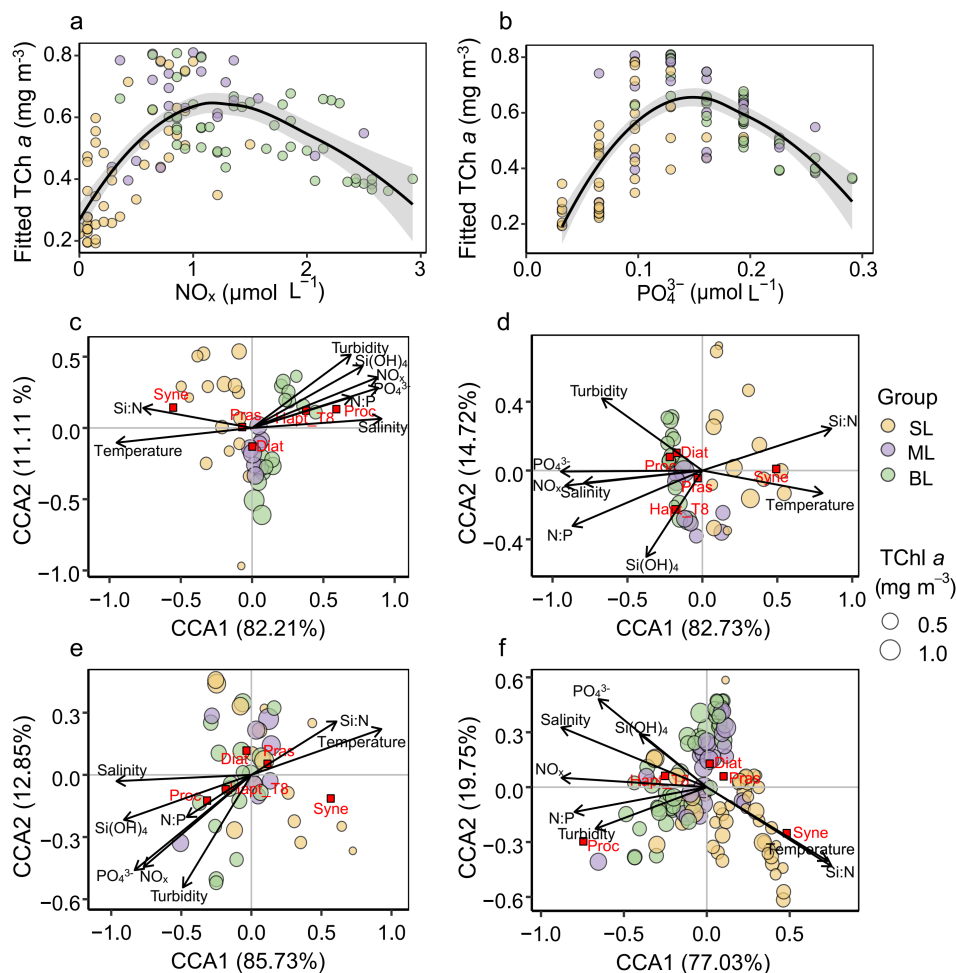


FIGURE 7

Relationships between TChl *a* and environmental factors, and CCA biplots for phytoplankton groups at stations Z1, Z2, and Z3. (A) Relationship between NO_x and TChl *a* fitted by generalized additive models (GAMs). (B) Relationship between PO_4^{3-} and TChl *a* fitted by GAMs. (C–F) Canonical correspondence analysis (CCA) biplots showing the relationships between dominant phytoplankton groups and key environmental variables at stations (C) Z1, (D) Z2, (E) Z3, and (F) combined data from stations Z1–Z3 (Z). The groups are color-coded by their corresponding vertical layers: surface layer (SL), mid-layer (ML), and bottom layer (BL). The size of the symbols represents the TChl *a* concentration.

temperatures, create highly favorable conditions for phytoplankton growth, particularly for diatoms (Harrison et al., 2008; Han et al., 2012; Tran et al., 2022). However, our study of the Pearl River plume as it extended into the Taiwan Strait revealed a complex narrative. Instead of promoting phytoplankton blooms, the plume exhibited significant nutrient depletion, leading to lower phytoplankton biomass and a shift in community composition. This finding contradicts the well-established notion that river plumes invariably boost coastal productivity by supplying essential nutrients. Our study sheds light on the intricate dynamics within the Taiwan Strait, where nutrient depletion coupled with vertical stratification significantly alters the ecological landscape. The intricate interactions between physical and biogeochemical processes revealed in this study challenge the simplistic view of river plumes as uniformly beneficial for phytoplankton growth and underscore the need for a more nuanced understanding of these systems.

4.1 Nutrient depletion and its consequences on phytoplankton biomass

As the Pearl River plume traveled from the estuary to the Taiwan Strait, it experienced substantial nutrient depletion, particularly in NO_x and PO_4^{3-} . Our data showed that NO_x concentrations in the surface layer of the Taiwan Strait were 26 and 6 times lower than those in the low-salinity plume and mesohaline plume stages observed on the northern South China Sea shelf, respectively (Tong et al., 2023). This dramatic decline was primarily due to the continuous uptake of nutrients by phytoplankton as the water mass moved seaward (Han et al., 2012).

The implications of this nutrient depletion were profound. The reduction in NO_x levels to concentrations below the half-saturation constants for phytoplankton uptake (0.5–2 μM ; Guillaud et al., 2000; Parekh et al., 2005) led to severe nitrogen limitation, a condition that persisted throughout the plume's extension into the Taiwan Strait

(Figure 7A). This limitation significantly suppressed phytoplankton biomass, as evidenced by the TChl *a* concentrations, which were four times lower in the surface layer of the Taiwan Strait compared to the average summer biomass in the region (Zhong et al., 2020). This finding contrasted sharply with the traditional view of river plumes as nutrient-rich zones that foster high phytoplankton productivity (Harrison et al., 2008; Weston et al., 2008).

Nutrient limitation, particularly nitrogen limitation, has been a well-documented phenomenon in other large river plumes, such as the Mississippi River plume, where it has been shown to reduce phytoplankton biomass as the water mass moves into oligotrophic waters (Turner and Rabalais, 2013). Similarly, nutrient depletion in the Amazon River plume has been associated with a shift from diatom dominance to smaller phytoplankton groups, such as picoplankton, due to reduced nutrient availability (Goes et al., 2014). Our study confirmed that the Pearl River plume behaved similarly as it extended into the Taiwan Strait, with nutrient depletion leading to reduced phytoplankton biomass and a shift in community composition.

4.2 Vertical stratification: a double-edged sword

The pronounced vertical stratification observed in the Taiwan Strait played a critical role in shaping phytoplankton dynamics. Our results indicated that the mid-layer, where the water mixed with ambient seawater, harbored higher nutrient concentrations and supported a deep chlorophyll maximum (DCM), a phenomenon commonly associated with stratified waters (Selmecky et al., 2016). This stratification created distinct vertical niches for different phytoplankton groups, with diatoms and prasinophytes dominating in the mid-layer, while *Synechococcus* was more prevalent in the surface layer (Figure 5).

However, this stratification also posed challenges. While the mid-layer provided a more favorable environment for phytoplankton growth due to higher nutrient availability, the surface layer was characterized by nutrient depletion and higher turbidity, which limited light penetration and further constrained phytoplankton growth (Rodrigues et al., 2009; Potes et al., 2012). In the bottom layer, light limitation became the dominant factor, as indicated by the lower phytoplankton biomass in this region (Figure 4).

The interplay between nutrient availability and light conditions across these layers illustrated the double-edged nature of stratification in the Taiwan Strait. On one hand, it supported the formation of a DCM and enhanced phytoplankton productivity in the mid-layer. On the other hand, it exacerbated nutrient and light limitations in the surface and bottom layers, leading to overall lower phytoplankton biomass in the Taiwan Strait compared to the northern South China Sea shelf stages (Tong et al., 2023). This stratification-induced niche differentiation has been observed in other systems as well, such as the Mississippi River plume, where vertical stratification influenced the spatial distribution of phytoplankton communities (Quigg et al., 2011).

4.3 Phytoplankton community composition: a shift from diatoms to *Synechococcus*

The shift in phytoplankton community composition observed in the Taiwan Strait further highlighted the unique dynamics of this region. In the nutrient-depleted surface layer, *Synechococcus* emerged as a dominant group, co-existing with diatoms that were likely transported from nutrient-rich regions closer to the estuary (Figure 5). This co-dominance contrasted with the traditional dominance of diatoms in estuarine and shelf environments, where nutrient levels are higher (Malone et al., 1983; Gomes et al., 2018).

Synechococcus, a picophytoplankton species adapted to oligotrophic conditions, thrived in the nutrient-poor surface layer, where it outcompeted larger phytoplankton like diatoms due to its lower nutrient requirements and higher growth rates at low nutrient concentrations (Agawin et al., 2000). The resilience of *Synechococcus* to nutrient limitation was evident in its negative correlation with nutrient concentrations (Figures 7C–F), suggesting that it was less impacted by the nutrient depletion that limited diatom growth in the surface waters.

While diatoms and *Synechococcus* dominated, the other identified phytoplankton groups, such as dinoflagellates, haptophytes, chlorophytes, and cryptophytes, were present but with lower pigment concentrations in the plume waters (Figure 5). This observation suggests that these groups were less competitive under the nutrient-depleted conditions in the surface layer, or they thrived in other layers where environmental factors such as light availability or turbulence were more favorable. For example, *Prochlorococcus* was predominantly found in the bottom layer (Figure 5), likely due to its preference for low light conditions (Partensky et al., 1999). Prasinophytes, although present in moderate quantities in the mid-layer, did not dominate due to their specific ecological niche, which is likely constrained by temperature and nutrient availability (Xiao et al., 2018; Zhong et al., 2020). Thus, the reduced focus on these groups reflects their minimal contribution to total phytoplankton biomass in the context of the plume's extension into the Taiwan Strait.

This shift towards a *Synechococcus*-dominated community in the surface layer has significant ecological implications. Picophytoplankton, including *Synechococcus*, are known to play a critical role in carbon cycling in oligotrophic oceans (Partensky et al., 1999). However, their dominance in the Taiwan Strait's surface waters represented a departure from the diatom-dominated communities typically associated with river plumes. This shift could have cascading effects on the marine food web, given the differences in trophic transfer efficiency and grazing pressures between picophytoplankton and larger phytoplankton like diatoms (Kjørboe, 1993; Moisan et al., 2010). Studies have shown that selective grazing by microzooplankton often targets *Synechococcus*, while diatoms, due to their larger size and tougher cell walls, are less susceptible to grazing (Christaki et al., 1999; Pančić et al., 2019).

4.4 Broader ecological and biogeochemical implications

The findings from our study suggested that the intrusion of the Pearl River plume into the Taiwan Strait did not follow the traditional paradigm of nutrient-rich river plumes enhancing coastal productivity. Instead, nutrient depletion, particularly nitrogen limitation, coupled with the region's vertical stratification, led to reduced phytoplankton biomass and a shift in community composition towards picophytoplankton dominance. These results contrast with previous studies conducted in the NSCS, where higher nutrient levels in the near-field plume supported diatom-dominated communities (Tong et al., 2023). Our focus on the far-field effects of the Pearl River plume in the Taiwan Strait reveals that, as the plume extends offshore, nutrient depletion becomes more pronounced, resulting in a community shift towards *Synechococcus* in the surface waters. These changes are likely to have broader implications for the biogeochemical cycling of carbon and nutrients in the region.

The observed nutrient limitations and their impact on phytoplankton biomass are consistent with trends observed in other large river systems, such as the Mississippi and Amazon Rivers, where similar patterns of nutrient depletion and changes in community composition have been reported (Turner and Rabalais, 2013; Goes et al., 2014). However, the unique physical and chemical characteristics of the Taiwan Strait, including its complex hydrodynamics and vertical stratification, created a distinct environment that further complicated the interactions between riverine inputs and marine ecosystems.

Future studies should focus on the long-term monitoring of nutrient dynamics and phytoplankton community composition in the Taiwan Strait to better understand the temporal variability and potential drivers of these observed patterns. Additionally, incorporating advanced techniques such as flow cytometry and molecular analysis could provide more detailed insights into the specific ecotypes of picophytoplankton and their responses to varying environmental conditions.

5 Conclusion

Our study reveals that the intrusion of the Pearl River plume into the Taiwan Strait presents a complex scenario that deviates from the traditional view of nutrient-rich river plumes enhancing coastal productivity. As the plume extends into the Taiwan Strait, significant nutrient depletion, particularly of NO_x , occurs in the surface waters, leading to severe nitrogen limitation and a consequent reduction in phytoplankton biomass. The vertical stratification within the Taiwan Strait further influences the spatial distribution of nutrients and light, creating distinct niches for different phytoplankton groups. This study highlights the shift from diatom dominance to a community increasingly dominated by *Synechococcus* in the nutrient-depleted surface layer, which has

important ecological implications for carbon cycling and food web dynamics in this region. Our findings challenge the conventional understanding of river plume dynamics and underscore the need for continued investigation into the biogeochemical processes governing coastal ecosystems, particularly in regions influenced by large river systems.

Data availability statement

The raw data supporting the conclusions of this article will be made available by the authors, without undue reservation.

Author contributions

ZT: Data curation, Visualization, Writing – original draft. CW: Data curation, Formal analysis, Investigation, Writing – original draft. LL: Data curation, Methodology, Writing – review & editing. LM: Conceptualization, Formal analysis, Funding acquisition, Writing – review & editing. BH: Formal analysis, Funding acquisition, Supervision, Writing – review & editing.

Funding

The author(s) declare that financial support was received for the research, authorship, and/or publication of this article. This work was funded by the National Natural Science Foundation of China (No. 42206140, 42130401, and 42141002) and the China Postdoctoral Science Foundation (No. 2021M702728).

Acknowledgments

We truly appreciate captains and crew of R/V *Yanping II* for their cooperation during the field cruises.

Conflict of interest

The authors declare that the research was conducted in the absence of any commercial or financial relationships that could be construed as a potential conflict of interest.

Publisher's note

All claims expressed in this article are solely those of the authors and do not necessarily represent those of their affiliated organizations, or those of the publisher, the editors and the reviewers. Any product that may be evaluated in this article, or claim that may be made by its manufacturer, is not guaranteed or endorsed by the publisher.

References

- Agawin, N. S. R., Duarte, C. M., and Agustí, S. (2000). Nutrient and temperature control of the contribution of picoplankton to phytoplankton biomass and production. *Limnol. Oceanogr.* 45, 591–600. doi: 10.4319/lo.2000.45.3.0591
- Bai, Y., Huang, T.-H., He, X., Wang, S.-L., Hsin, Y.-C., Wu, C.-R., et al. (2015). Intrusion of the Pearl River plume into the main channel of the Taiwan Strait in summer. *J. Sea Res.* 95, 1–15. doi: 10.1016/j.seares.2014.10.003
- Cai, W.-J., Dai, M., Wang, Y., Zhai, W., Huang, T., Chen, S., et al. (2004). The biogeochemistry of inorganic carbon and nutrients in the Pearl River estuary and the adjacent Northern South China Sea. *Continental Shelf Res.* 24, 1301–1319. doi: 10.1016/j.csr.2004.04.005
- Christaki, U., Jacquet, S., Dolan, J. R., Vaulot, D., and Rassoulzadegan, F. (1999). Growth and grazing on *Prochlorococcus* and *Synechococcus* by two marine ciliates. *Limnol. Oceanogr.* 44, 52–61. doi: 10.4319/lo.1999.44.1.0052
- Dai, M., Zhai, W., Cai, W.-J., Callahan, J., Huang, B., Shang, S., et al. (2008). Effects of an estuarine plume-associated bloom on the carbonate system in the lower reaches of the Pearl River estuary and the coastal zone of the northern South China Sea. *Continental Shelf Res.* 28, 1416–1423. doi: 10.1016/j.csr.2007.04.018
- Field, C. B., Behrenfeld, M. J., Randerson, J. T., and Falkowski, P. (1998). Primary production of the biosphere: Integrating terrestrial and oceanic components. *Science* 281, 237–240. doi: 10.1126/science.281.5374.237
- Gao, N., Ma, Y., Zhao, M., Zhang, L., Zhan, H., Cai, S., et al. (2020). Quantile analysis of long-term trends of near-surface chlorophyll-*a* in the Pearl River Plume. *Water* 12, 1662. doi: 10.3390/w12061662
- Goes, J. I., Gomes, H., do, R., Chekalyuk, A. M., Carpenter, E. J., Montoya, J. P., et al. (2014). Influence of the Amazon River discharge on the biogeography of phytoplankton communities in the western tropical north Atlantic. *Prog. Oceanogr.* 120, 29–40. doi: 10.1016/j.pocean.2013.07.010
- Gomes, H., do, R., Xu, Q., Ishizaka, J., Carpenter, E. J., Yager, P. L., et al. (2018). The influence of riverine nutrients in niche partitioning of phytoplankton communities—a contrast between the Amazon River Plume and the Changjiang (Yangtze) River diluted water of the East China Sea. *Front. Mar. Sci.* 5. doi: 10.3389/fmars.2018.00343
- Guillaud, J.-F., Andrieux, F., and Menesguen, A. (2000). Biogeochemical modelling in the Bay of Seine (France): an improvement by introducing phosphorus in nutrient cycles. *Journal of Marine Systems* 25, 369386. doi: 10.1016/S0924-7963(00)00028-2
- Han, A., Dai, M., Kao, S.-J., Gan, J., Li, Q., Wang, L., et al. (2012). Nutrient dynamics and biological consumption in a large continental shelf system under the influence of both a river plume and coastal upwelling. *Limnol. Oceanogr.* 57, 486–502. doi: 10.4319/lo.2012.57.2.0486
- Harrison, P. J., Yin, K., Lee, J. H. W., Gan, J., and Liu, H. (2008). Physical–biological coupling in the pearl river estuary. *Continental Shelf Res.* 28, 1405–1415. doi: 10.1016/j.csr.2007.02.011
- Hong, H., Chai, F., Zhang, C., Huang, B., Jiang, Y., and Hu, J. (2011). An overview of physical and biogeochemical processes and ecosystem dynamics in the Taiwan Strait. *Continental Shelf Res.* 31, S3–S12. doi: 10.1016/j.csr.2011.02.002
- Huang, T.-H., Chen, C.-T. A., Zhang, W.-Z., and Zhuang, X.-F. (2015). Varying intensity of Kuroshio intrusion into Southeast Taiwan Strait during ENSO events. *Continental Shelf Res.* 103, 79–87. doi: 10.1016/j.csr.2015.04.021
- Kjørboe, T. (1993). “Turbulence, phytoplankton cell size, and the structure of pelagic food webs,” in *Advances in marine biology* eds. J. H. S. Blaxter and A. J. Southward (Academic Press), 1–72. doi: 10.1016/S0065-2881(08)60129-7
- Latasa, M. (2007). Improving estimations of phytoplankton class abundances using CHEMTAX. *Mar. Ecol. Prog. Ser.* 329, 13–21. doi: 10.3354/meps329013
- Lu, Z., and Gan, J. (2015). Controls of seasonal variability of phytoplankton blooms in the Pearl River Estuary. *Deep Sea Res. II* 117, 86–96. doi: 10.1016/j.dsr2.2013.12.011
- Malone, T. C., Falkowski, P. G., Hopkins, T. S., Rowe, G. T., and Whitedge, T. E. (1983). Mesoscale response of diatom populations to a wind event in the plume of the Hudson River. *Deep Sea Res. II* 30, 149–170. doi: 10.1016/0198-0149(83)90066-3
- Moisan, T. A., Blattner, K. L., and Mankinen, C. P. (2010). Influences of temperature and nutrients on *Synechococcus* abundance and biomass in the southern Mid-Atlantic Bight. *Continental Shelf Res.* 30, 1275–1282. doi: 10.1016/j.csr.2010.04.005
- Mouriño-Carballido, B., Hojas, E., Cermeño, P., Chouciño, P., Fernández-Castro, B., Latasa, M., et al. (2016). Nutrient supply controls picoplankton community structure during three contrasting seasons in the northwestern Mediterranean Sea. *Mar. Ecol. Prog. Ser.* 543, 1–19. doi: 10.3354/meps11558
- Pančić, M., Torres, R. R., Almeda, R., and Kjørboe, T. (2019). Silicified cell walls as a defensive trait in diatoms. *Proc. R. Soc. B* 286, 20190184. doi: 10.1098/rspb.2019.0184
- Parekh, P., Follows, M. J., and Boyle, E. A. (2005). Decoupling of iron and phosphate in the global ocean. *Global Biogeochem. Cycles* 19, 2. doi: 10.1029/2004GB002280
- Partensky, F., Blanchot, J., and Vaulot, D. (1999). Differential distribution and ecology of *Prochlorococcus* and *Synechococcus* in oceanic waters: a review. *Bull. Institut Océanographique Monaco-Numero Special* 17, 457–476.
- Potes, M., Costa, M. J., and Salgado, R. (2012). Satellite remote sensing of water turbidity in Alqueva reservoir and implications on lake modelling. *Hydrol. Earth Syst. Sci.* 16, 1623–1633. doi: 10.5194/hess-16-1623-2012
- Quigg, A., Sylvan, J. B., Gustafson, A. B., Fisher, T. R., Oliver, R. L., Tozzi, S., et al. (2011). Going west: nutrient limitation of primary production in the Northern Gulf of Mexico and the importance of the Atchafalaya River. *Aquat. Geochem.* 17, 519–544. doi: 10.1007/s10498-011-9134-3
- R Core Team (2022). *R: A language and environment for statistical computing* (R Foundation for Statistical Computing). Available at: www.r-project.org/.
- Rodrigues, R. P., Knoppers, B. A., de Souza, W. F. L., and Santos, E. S. (2009). Suspended matter and nutrient gradients of a small-scale river plume in Sepetiba Bay, SE-Brazil. *Arch. Biol. Technol.* 52, 503–512. doi: 10.1590/S1516-89132009000200030
- Selmeczy, G. B., Tapolczai, K., Casper, P., Krienitz, L., and Padisák, J. (2016). Spatial- and niche segregation of DCM-forming cyanobacteria in Lake Stechlin (Germany). *Hydrobiologia* 764, 229–240. doi: 10.1007/s10750-015-2282-5
- Shen, P.-P., Li, G., Huang, L.-M., Zhang, J.-L., and Tan, Y.-H. (2011). Spatio-temporal variability of phytoplankton assemblages in the Pearl River estuary, with special reference to the influence of turbidity and temperature. *Continental Shelf Res.* 31, 1672–1681. doi: 10.1016/j.csr.2011.07.002
- Tong, Z., Ma, L., Cai, S., Wang, L., Xiao, W., Huang, B., et al. (2023). Responses of phytoplankton communities to the effect of both river plume and coastal upwelling. *J. Geophys. Res.: Biogeosci.* 128, e2023JG007486. doi: 10.1029/2023JG007486
- Tran, T. H. Y., Tran, T. T., Nguyen, T. M. Y., Ngo, X. Q., Nguyen, X. D., and Pham, T. L. (2022). Seasonal changes in phytoplankton assemblages and environmental variables in highly turbid tropical estuaries of the Mekong River, Vietnam. *Environ. Monit. Assess.* 194, 776. doi: 10.1007/s10661-022-10181-x
- Turner, R., and Rabalais, N. (2013). Nitrogen and phosphorus phytoplankton growth limitation in the northern Gulf of Mexico. *Aquat. Microb. Ecol.* 68, 159–169. doi: 10.3354/ame01607
- Vic, C., Berger, H., Tréguier, A.-M., and Couvelard, X. (2014). Dynamics of an equatorial river plume: theory and numerical experiments applied to the Congo Plume case. *J. Phys. Oceanogr.* 44, 980–994. doi: 10.1175/JPO-D-13-0132.1
- Wang, J., Hong, H., Jiang, Y., Chai, F., and Yan, X.-H. (2013). Summer nitrogenous nutrient transport and its fate in the Taiwan Strait: A coupled physical-biological modeling approach. *J. Geophys. Res.: Oceans* 118, 4184–4200. doi: 10.1002/jgrc.20300
- Wang, L., Huang, B., Liu, X., and Xiao, W. (2015). The modification and optimizing of the CHEMTAX running in the South China Sea. *Acta Oceanol. Sin.* 34, 124–131. doi: 10.1007/s13131-015-0621-z
- Weston, K., Greenwood, N., Fernand, L., Pearce, D. J., and Sivy, D. B. (2008). Environmental controls on phytoplankton community composition in the Thames plume, U.K. *J. Sea Res.* 60, 246–254. doi: 10.1016/j.seares.2008.09.003
- Wu, K., Dai, M., Li, X., Meng, F., Chen, J., and Lin, J. (2017). Dynamics and production of dissolved organic carbon in a large continental shelf system under the influence of both river plume and coastal upwelling: Dynamics and production of dissolved organic carbon. *Limnol. Oceanogr.* 62, 973–988. doi: 10.1002/lno.10479
- Xiao, W., Wang, L., Laws, E., Xie, Y., Chen, J., Liu, X., et al. (2018). Realized niches explain spatial gradients in seasonal abundance of phytoplankton groups in the South China Sea. *Prog. Oceanogr.* 162, 223–239. doi: 10.1016/j.pocean.2018.03.008
- Yin, K., Qian, P., Wu, M., Chen, J., Huang, L., Song, X., et al. (2001). Shift from P to N limitation of phytoplankton growth across the Pearl River estuarine plume during summer. *Mar. Ecol. Prog. Ser.* 221, 17–28. doi: 10.3354/meps221017
- Yin, K., Song, X., Sun, J., and Wu, M. C. S. (2004). Potential P limitation leads to excess N in the pearl river estuarine coastal plume. *Continental Shelf Res.* 24, 1895–1907. doi: 10.1016/j.csr.2004.06.014
- Zhong, Y., Hu, J., Laws, E. A., Liu, X., Chen, J., and Huang, B. (2019). Plankton community responses to pulsed upwelling events in the southern Taiwan Strait. *ICES J. Marine Sci.* 76, 2374–2388. doi: 10.1093/icesjms/fsz142
- Zhong, Y., Liu, X., Xiao, W., Laws, E. A., Chen, J., Wang, L., et al. (2020). Phytoplankton community patterns in the Taiwan Strait match the characteristics of their realized niches. *Prog. Oceanogr.* 186, 102366. doi: 10.1016/j.pocean.2020.102366